Design optimization of piezoresistive cantilevers for force sensing in air and water

Joseph C. Doll, Sung-Jin Park, and Beth L. Pruitt[a)]
Department of Mechanical Engineering, Stanford University, Stanford, California 94305-4040, USA

(Received 6 May 2009; accepted 13 August 2009; published online 23 September 2009)

Piezoresistive cantilevers fabricated from doped silicon or metal films are commonly used for force, topography, and chemical sensing at the micro- and macroscales. Proper design is required to optimize the achievable resolution by maximizing sensitivity while simultaneously minimizing the integrated noise over the bandwidth of interest. Existing analytical design methods are insufficient for modeling complex dopant profiles, design constraints, and nonlinear phenomena such as damping in fluid. Here we present an optimization method based on an analytical piezoresistive cantilever model. We use an existing iterative optimizer to minimimize a performance goal, such as minimum detectable force. The design tool is available as open source software. Optimal cantilever design and performance are found to strongly depend on the measurement bandwidth and the constraints applied. We discuss results for silicon piezoresistors fabricated by epitaxy and diffusion, but the method can be applied to any dopant profile or material which can be modeled in a similar fashion or extended to other microelectromechanical systems. © *2009 American Institute of Physics*. [doi:10.1063/1.3224965]

I. INTRODUCTION

Microfabricated silicon cantilevers are widely used in force,[1,2] topography,[3] and biochemical sensing[4] applications by transducing a signal via cantilever deflection. There are numerous techniques to detect cantilever bending, but the most common approaches are off-chip optical sensing[3] and on-chip electronic sensing using piezoresistive strain gauges.[5,6] Electronic sensing scales well to large arrays,[7] high frequencies,[8] and situations where optics are inconvenient.[9] With proper design, the resolution of piezoresistive cantilevers is comparable to optical detection.[5] However, the design methods used to date[10] are often misapplied in practice and are not readily generalizable to situations beyond epitaxial silicon piezoresistors in air.

Tradeoffs are a major part of piezoresistive cantilever design. In optimizing force resolution, for example, the cantilever design parameters must be properly chosen to balance the force sensitivity and noise sources of the cantilever given a set of design and operating constraints. The duration and time resolution of the measurement are particularly important and determine the frequency range over which the cantilever must operate. Prior publications on the design of piezoresistive cantilevers have presented analytically derived results for a single frequency range[10] or performed local optimization on a single variable at a time.[11] The results from Ref. 10 were derived for a 1 μm thick epitaxial cantilever operating in air from 10 Hz to 1 kHz. However, they have been directly applied to other fabrication methods[12] and measurement bandwidths,[13] but do not provide optimized performance, in general.

Analytical approaches are difficult to apply to nonlinear phenomena such as fluid damping which are more readily modeled numerically. In contrast, multivariate design optimization has been shown to yield improved performance in many applications, including piezoresistive microphones,[14] and more effectively accounts for uncertainty.[15] Although epitaxial piezoresistors are straightforward to analyze, the dopant profiles from other methods such as diffusion and ion implantation are not as easily manipulated. In summary, existing design methodologies are not sufficient for cases such as high bandwidth cantilevers operating in liquid, particularly for doping methods other than epitaxy, and there is a need for a more general method which can combine analytical and numerical modeling.

In this work we combine a primarily analytical model for cantilever performance with an iterative optimizer to investigate the influence of design variables and constraints on cantilever performance. We particularly emphasize high frequency force detection in air and liquid environments. Results are primarily discussed for epitaxial piezoresistors, but we also extended the code to diffusion to demonstrate its flexibility. Additionally, we emphasize single crystal silicon piezoresistors but it is possible to apply the code to polysilicon or metal piezoresistors as well. We have made the design and optimization code freely available as an open source project and designed it to be useful in practice for other researchers. The design approach we describe is general and can easily be applied to other loading conditions,[4] sensor geometries,[16] and transduction methods.[17,18]

II. METHOD

The cantilever geometry used in this work is shown in Fig. 1. The cantilever is of a split-leg design; two separate legs each of length l_{pr} and width $w/2$ form a loop to define the piezoresistor. The cantilever extends beyond the end of

[a)]Author to whom correspondence should be addressed. Present address: 496 Lomita Mall, Durand Building, Rm. 213, Stanford, California 94305-4040. Tel.: 650-723-4559. FAX: 650-725-1587. Electronic mail: pruitt@stanford.edu.

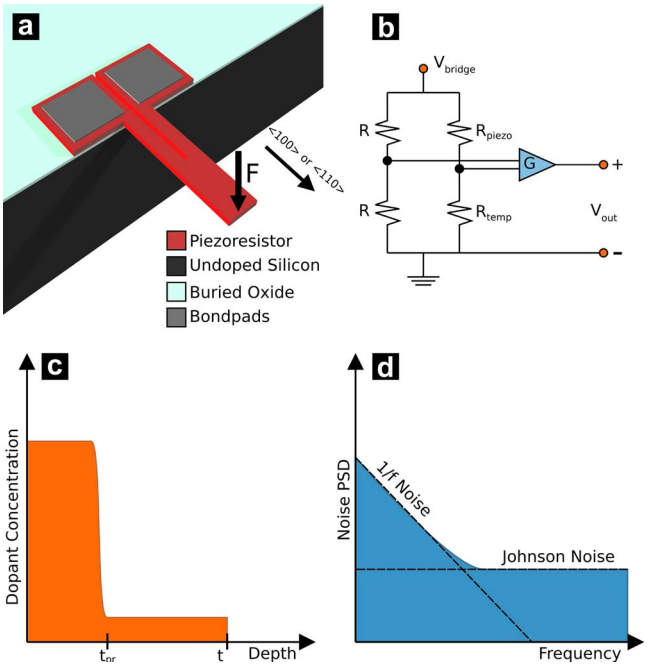

FIG. 1. (Color online) (a) Cantilever schematic. The cantilever has a total length l, width w, and thickness t. The piezoresistor loop is formed by the two legs, each of width $w/2$, separated by a negligible gap. The piezoresistor is oriented in the $\langle 110\rangle$ or $\langle 100\rangle$ for a p-type or n-type piezoresistor, respectively, in order to maximize sensitivity. (b) The change in resistance of the piezoresistor with applied force is read out with a Wheatstone bridge. Two piezoresistors are included in the bridge for reduced sensitivity to temperature change and other disturbances. (c) The piezoresistor can be formed using numerous methods which yield an electrically active dopant concentration which varies with depth. (d) Noise PSD of the piezoresistor is composed of $1/f$ (Hooge) noise and Johnson noise. The choice of cantilever design determines the corner frequency at which piezoresistor noise transitions from $1/f$ dominated to Johnson noise dominated.

the piezoresistor to a total length l. The thickness t is uniform along the length. The gap between the legs is assumed to be negligibly wide, and the cantilever can be approximated to have a uniform width w. This design is straightforward to analyze and fabricate using epitaxy, diffusion, or ion implantation. It is worth emphasizing that the piezoresistor should occupy the entire width of the cantilever, as assumed throughout this analysis. As the piezoresistor becomes narrower than the cantilever, both the Johnson noise and Hooge noise increase while the sensitivity remains constant.

A. Force sensitivity

The system is modeled as a linear elastic cantilever beam with a point load applied at the tip via Euler–Bernoulli beam theory. We assume negligible transverse stress in the cantilever legs, and the longitudinal stress induced as a function of distance x from the base and z from the neutral axis of the cantilever is

$$\sigma = \frac{12F(l-x)z}{wt^3}. \tag{1}$$

The longitudinal stress induced by a point load is zero at the neutral axis and varies linearly through the cantilever thickness, thus the stress experienced by the piezoresistor varies by position. Stress is independent of the cantilever mechanical properties and is solely dependent on geometry, which is a consideration for the choice of dopant type and will be discussed later.

TABLE I. Optimized p-type epitaxial piezoresistive cantilever designs. The values for f_{min} and f_{max} are provided to the optimizer, while constraints are placed on t ($\geqslant$1 μm or $\geqslant$10 μm), n ($\leqslant 4.4\times10^{19}$), f_0 ($\geqslant 5f_{max}$), V_{bridge} ($\leqslant$10 V), and W ($\leqslant$2.5 mW). The other parameters are calculated by the optimization routine.

Cantilever	1	2	3	4
Ambient	Vacuum	Vacuum	Vacuum	Water
f_{min} (Hz)	1	1	1	1
f_{max} (kHz)	1	1	100	100
l (μm)	1658	524	52.4	40.8
w (μm)	20	2	2	2
t (μm)	10	1	1	1
l_{pr}/l	0.25	0.29	0.40	0.43
t_{pr}/t	0.11	0.33	0.19	0.20
n (cm^{-3})	6.0×10^{18}	4.4×10^{19}	4.4×10^{19}	4.4×10^{19}
F_{min} (pN)	202	2.6	123	169
S_F (V/N)	2.3×10^{3}	4.1×10^{5}	3.5×10^{4}	2.4×10^{4}
β^*	0.61	0.34	0.41	0.41
$\overline{V_{noise}}$ (V)	4.6×10^{-7}	1.1×10^{-6}	4.4×10^{-6}	4.0×10^{-6}
$\overline{V_H}/\overline{V_J}$	0.61	1.42	0.99	1.07
f_{corner} (kHz)	0.05	0.29	8.5	9.8
N	5.6×10^{10}	4.4×10^{9}	3.5×10^{8}	3.1×10^{8}
k (N/m)	0.19	5.9×10^{-4}	0.59	1.24
f_0 (kHz)	5	5	500	825
f_{fluid} (kHz)	2.9	0.7	286	500
V_{bridge} (V)	9.6	10	7.6	6.7
R (kΩ)	9.2	23.4	5.7	4.5
W (mW)	2.5	1.1	2.5	2.5

If the cantilever length is comparable to its width, transverse stress starts to become significant and must be considered in the design. The transverse stress affects both the piezoresistor sensitivity and the beam mechanics. The effect on sensitivity can be incorporated through simulation,[19] while the beam mechanics can be modified by using the adjusted plate modulus to calculate the beam stiffness, $E/(1-\nu^2)$, where E is the elastic modulus and ν is Poisson's ratio of the beam material.[20]

The stress field is transduced by the piezoresistive effect as a change in resistivity, according to

$$\frac{\Delta\rho}{\rho} = \pi_l\sigma_l + \pi_t\sigma_t, \tag{2}$$

where π_l and π_t are the longitudinal and transverse piezoresistive coefficients, while σ_l and σ_t are the longitudinal and transverse stress components where the piezoresistor is situated. The piezoresistive effect is assumed to be linear, which is accurate to 0.1% and 1% for stresses of 15.3 and 139 MPa of stress.[21] This corresponds to less than 0.1% nonlinearity for a dynamic range of 40 dB for the designs discussed later in Table I.

The piezoresistance factor is assumed to be independent of temperature because the dopant concentrations utilized here are fairly high.[22] However, the piezoresistance factor could be coupled to temperature based on experimental data[23] for both sensitivity and noise analysis. Although this

extension would be difficult analytically, it is straightforward with the numerical approach used here. The piezoresistive coefficient for boron doped piezoresistors is taken from Harley's fit of experimental data,[24]

$$\pi_l = P\pi_0, \tag{3}$$

where $\pi_0 = 72 \times 10^{-11}$ Pa^{-1} for p-type piezoresistors oriented in the ⟨110⟩ direction and

$$P = \log_{10}\left(\frac{b}{n}^a\right), \tag{4}$$

where $a = 0.2014$, $b = 1.53 \times 10^{22}$ cm^{-3}, and n is the dopant concentration. If the piezoresistor is uniformly doped, infinitely thin, and located at the surface of the cantilever where the stress is maximized, the fractional change in resistance is[25]

$$\frac{\Delta R}{R} = \frac{6\pi_l(l - l_{\mathrm{pr}}/2)}{wt^2}F, \tag{5}$$

where l, w, and t are the cantilever dimensions and l_{pr} is the length of the piezoresistor as noted earlier. In practice, these assumptions overpredict cantilever sensitivity due to the finite thickness of the piezoresistor [Fig. 1(c)]. Therefore, we introduce an efficiency factor β^* as in Ref. 26, which accounts for the finite thickness of the piezoresistor and proportionally reduces the fractional change in resistance,

$$\beta^* = \frac{2}{t}\frac{\int_{-t/2}^{t/2} q\mu n P z dz}{\int_{-t/2}^{t/2} q\mu n dz}, \tag{6}$$

where the majority carrier mobility μ and piezoresistive coefficient P are both functions of dopant concentration n, which varies with depth z. In the case of a uniformly doped piezoresistor with finite thickness t_{pr}, β^* simplifies to

$$\beta^* = P\left(1 - \frac{t_{\mathrm{pr}}}{t}\right). \tag{7}$$

A simplified form was first derived in Ref. 5 before being extended to a dopant profile with varying concentration in Ref. 26. A Wheatstone bridge is commonly used to transduce the change in resistance to a voltage. Although a bridge reduces the sensitivity of the system ($V_{\mathrm{out}}/V_{\mathrm{bridge}} \approx \Delta R/4R$), it is straightforward to implement. For all sensitivity and noise calculations, we assume a quarter-active Wheatstone bridge with an additional temperature compensation piezoresistor as shown in Fig. 1(b). The overall voltage sensitivity is given as

$$S_F = \frac{\Delta V}{F} = \frac{3\pi_0(l - l_{\mathrm{pr}}/2)}{2wt^2}V_{\mathrm{bridge}}\beta^*\gamma, \tag{8}$$

where γ is the ratio of the piezoresistor resistance to the total resistance measured. Resistance that does not contribute to the change in resistance with applied force, such as contact resistance and conducting traces, acts to reduce system sensitivity and increase noise, both by the increased resistance and regions of high current density which contribute to $1/f$ noise. We assume $\gamma = 1$ for simplicity.

The piezoresistive coefficient varies according to the dopant type and the crystallographic orientation of the current flow relative to the applied stress. For a p-type dopant, the direction of maximum piezoresistive coefficient is the ⟨110⟩ direction, while for n-type dopants the optimum direction of stress and current is the ⟨100⟩ direction.

The flow of current transverse to the longitudinal stress at the end of the piezoresistor results in a reduction in sensitivity because $\pi_T \approx -\pi_L$ for p-type piezoresistors in the ⟨110⟩ direction. Generally the piezoresistor is much longer than it is wide and the turn at the end of the piezoresistor is insignificant.[25] The contribution of the transverse current can be calculated as

$$\left|\frac{\Delta R_T}{\Delta R_L}\right| \approx \frac{w\left(\frac{1}{a} - 1\right)}{l\left(1 - \frac{a}{2}\right)}, \tag{9}$$

where $a = l_{\mathrm{pr}}/l$. The effect is generally small (for $w/l = 1/50$ and $a = 0.3$, $|\Delta R_T/\Delta R_L| = 5\%$) and we neglect it in the present analysis.

As a sensitivity analysis example, consider cantilever 1 in Table I. The cantilever is 10 μm thick, 20 μm wide, and 1658 μm long, with a piezoresistor that is 1.1 μm thick and 415 μm long and doped to 6×10^{18} cm^{-3}. The efficiency factor and sensitivity can be calculated from Eqs. (7) and (8) to be $\beta^* = 0.61$ and $S_F = 2287$ V/N.

B. Noise

Piezoresistive cantilever performance is limited by three primary sources of noise: Johnson, $1/f$ and amplifier. Thermomechanical noise[27,28] and fluid damping noise[29] are not included in the present analysis but should be considered in certain applications, such as those requiring subpiconewton force resolution.[30] These other noise sources will be briefly discussed at the end of this section.

1. Johnson noise

Johnson noise is the result of the thermal motion of carriers within resistive elements and is independent of frequency[31] [Fig. 1(d)]. The "white noise" is dependent on the resistance R and temperature T of the resistor, and the noise power spectral density (V^2/Hz) for a single resistor is

$$\overline{S_J^2} = 4k_bTR, \tag{10}$$

where k_b is Boltzmann's constant. The Johnson noise of a balanced Wheatstone bridge is equal to the Johnson noise of a single resistor, so that the overall Johnson noise power of the Wheatstone bridge in the frequency band f_{min} to f_{max} is

$$\overline{V_J^2} = 4k_bTR(f_{\mathrm{max}} - f_{\mathrm{min}}). \tag{11}$$

The resistance of an epitaxial piezoresistor can be approximated as

$$R = \rho\frac{4l_{\mathrm{pr}}}{wt_{\mathrm{pr}}}, \tag{12}$$

where ρ is the resistivity of the piezoresistor. Resistivity varies according to dopant concentration n as

$$\rho = \frac{1}{q\mu n}, \tag{13}$$

where μ is the concentration dependent majority carrier mobility.[32]

Once again using cantilever 1 in Table I as an example, the resistance is calculated from Eqs. (12) and (13) ($R = 9.2\ \mathrm{k}\Omega$). Combining the resistance with $f_{\min}$ (1 Hz) and $f_{\max}$ (1 kHz), the integrated Johnson noise power [Eq. (11)] is $1.52 \times 10^{-13}\ \mathrm{V}^2$, or equivalently, the rms Johnson noise voltage is 3.9×10^{-7} V.

2. Hooge noise

The dominant $1/f$ noise source in silicon piezoresistors is Hooge noise.[10] Hooge noise is a fluctuation in resistor conductance which can be attributed to defects in the bulk of the material.[33] In contrast with Johnson noise, which is a voltage noise, Hooge noise is a conductivity noise and the noise voltage depends on the bias voltage. The noise is independent of the resistance and is inversely proportional to the number of carriers in the resistor. The voltage power spectral density of a single piezoresistor has been empirically modeled as

$$\overline{S_H^2} = \frac{\alpha V_{\mathrm{bias}}^2}{Nf}, \tag{14}$$

where $V_{\mathrm{bias}} = V_{\mathrm{bridge}}/2$ is the piezoresistor bias voltage, N is the total number of carriers in the resistor, and f is the frequency [Fig. 1(d)]. The parameter α is an experimentally measured value that is dependent on the crystal lattice quality. Ion implantation causes damage to the crystal that must be annealed out, and it has been observed that α decreases with the mean diffusion length ($\sqrt{Dt}$) of the dopant atoms during the anneal. For epitaxial piezoresistors, $\alpha = 10^{-5}$ is typical[24] and we use this value in the presented analysis. However, values of α as low as 10^{-7} have been reported for implanted piezoresistors[34] and specific fabrication processes (e.g., reactive ion etching) have been shown to affect the $1/f$ noise performance of piezoresistors.[35]

The Wheatstone bridge is composed of two piezoresistors which are uncorrelated $1/f$ noise sources so the $1/f$ noise power is increased by a factor of 2 (voltage increased by $\sqrt{2}$), and the integrated voltage noise power is

$$\overline{V_H^2} = \frac{\alpha V_{\mathrm{bridge}}^2}{2N} \ln\left(\frac{f_{\max}}{f_{\min}}\right). \tag{15}$$

$1/f$ noise is dependent on frequency and its integrated power is constant per decade. The number of carriers can be calculated from the dopant concentration profile and piezoresistor volume assuming a constant current density,[24] and for an epitaxial piezoresistor is

$$N = n l_{\mathrm{pr}} w t_{\mathrm{pr}}. \tag{16}$$

Using cantilever 1 in Table I as an example, the number of carriers can be calculated from Eq. (16) to be $N = 5.6 \times 10^{10}$. Using N, V_{bridge} (9.6 V), $f_{\min}$, and $f_{\max}$, we can calculate the Hooge noise power [Eq. (15)] to be $5.8 \times 10^{-14}\ \mathrm{V}^2$, or a noise voltage of 2.4×10^{-7} V. Note that this is slightly less than the Johnson noise power.

3. Amplifier noise

The typical measurement circuit for a piezoresistive sensor includes a Wheatstone bridge, instrumentation amplifier, and electronic filters [Fig. 1(b)]. With proper choice of bridge resistors and filters, only the instrumentation amplifier noise need be considered. Specifically, the additional resistors in the Wheatstone bridge should have low $1/f$ noise and be less than or equal in resistance to the piezoresistors. The electromagnetic shielding and the noise characteristics of the other electronic components in the circuit must also be considered. We select a low noise instrumentation amplifier (INA103, Texas Instruments) with sufficient bandwidth for high frequency force sensing (−3 dB bandwidth of 800 kHz, $G = 100$), and an input referred voltage noise of approximately

$$\overline{V_A^2} = C_J^2(f_{\max} - f_{\min}) + C_H^2 \ln\left(\frac{f_{\max}}{f_{\min}}\right), \tag{17}$$

where $C_J = 1.8\ \mathrm{nV}/\sqrt{\mathrm{Hz}}$ and $C_H = 10$ nV with a gain of 100.

In a measurement bandwidth from 1 Hz to 1 kHz, this translates to a noise power of $4 \times 10^{-15}\ \mathrm{V}^2$ or a rms noise voltage of 6.3×10^{-8} V. This is four to six times less than the Johnson and Hooge noise sources, although the relative magnitude of the noise sources depends on the cantilever design and optimization constraints which will be discussed later.

4. Other noise sources

As noted previously, thermomechanical and fluid damping noise can be significant for certain applications. For the optimization design space explored in this paper they are not significant, but we will briefly discuss them here. Whereas thermomechanical noise is intrinsic to the cantilever and is caused by the Brownian motion of the silicon atoms, fluid damping noise is caused by the Brownian motion of the immersing fluid. The thermomechanical noise force can be calculated from

$$F_{\mathrm{th}} = \sqrt{\frac{2kk_bT(f_{\max} - f_{\min})}{\pi f_0 Q}}, \tag{18}$$

where k and Q are the spring constant and mechanical quality factor of the cantilever, respectively. For the example cantilever design followed through the previous sections (cantilever 1 in Table I) and conservatively assuming $Q = 100$, this translates to a force of 1 pN.

The fluid damping noise force can be calculated from the equipartition theorem by equating the thermal energy of the fluid molecules with the elastic bending energy of the cantilever,

$$F_d = \sqrt{k_b kT}. \tag{19}$$

For the example cantilever this corresponds for a noise force contribution of 0.3 pN.

Both noise sources are significantly less than that of the electronic noise sources for most microscale cantilever designs. In comparison with the electronic noise limited force

resolution of the example cantilever (202 pN, discussed in Sec. II C), thermomechanical and fluid damping noise are insignificant.

C. Force resolution

The overall root mean square voltage noise is the sum of the uncorrelated noise sources described in the previous sections,

$$\overline{V_{\text{noise}}} = \sqrt{\overline{V_J^2} + \overline{V_H^2} + \overline{V_A^2}}. \tag{20}$$

The ratio of V_J to V_H depends on the cantilever design and the measurement frequency range. For a cantilever optimized for broadband force sensing, we show in Sec. III B that $V_J \approx V_H$.

The minimum resolvable force can be calculated from the integrated voltage noise and the force sensitivity of the device according to

$$F_{\text{min}} = \frac{\overline{V_{\text{noise}}}}{S_F}. \tag{21}$$

The goal of the designer is to minimize F_{min} by optimizing the ratio of $\overline{V_{\text{noise}}}$ to S_F, which can be calculated from the cantilever design parameters. The components of this model are well established,[2,10] but we verified the accuracy of the model by comparing it with the experimental data presented in Ref. 24 for a 90 nm thick epitaxial piezoresistor. The force resolution, integrated noise, and stiffness all agree to within 10% of the reported values, e.g., a force resolution of 0.5 pN is reported and we calculate a value of 0.56 pN.

Again considering cantilever 1 in Table I, we can calculate the total noise magnitude from Equation (20) ($\overline{V_{\text{noise}}} = 4.6 \times 10^{-7}$). Combining the force sensitivity and Eq. (21), we calculate a force resolution of 202 pN.

D. Bandwidth

The measurement bandwidth of a cantilever is limited by its mechanical resonance. The frequency components of a force signal near the resonant modes of the cantilever are amplified, which can be beneficial in the case of resonant mode detection or must be avoided in closed loop force control applications. A flat frequency response is beneficial for passive force sensing, where it reduces calibration to a single sensitivity value rather than a frequency dependent one, and for force feedback applications, where the resonant modes must be compensated to preserve stability. The first resonant mode of a cantilever can be derived from the Euler–Bernoulli beam equation as[20]

$$f_0 = \frac{1}{2\pi}\sqrt{\frac{k}{m_{\text{eff}}}} \approx \frac{1}{\pi}\sqrt{\frac{E}{\rho_c}}\frac{t}{L^2}. \tag{22}$$

where ρ_c is the density of the cantilever beam. Additionally, it is important that the cantilever is stiffer in the transverse in-plane direction than the out-of-plane direction, or equivalently, that the first out-of-plane resonant mode is at a lower frequency than the first transverse in-plane mode.

The frequency response of the cantilever in fluid is modeled based on Van Eysden and Sader.[36] Classical beam theory is combined with solution of the linearized Navier–Stokes equations to predict the frequency response of a cantilever for arbitrary mode order. Assumptions of the model include a rectangular, uniform cross section, and $l \gg w \gg t$. In the case of small dissipative effects ($Q \gg 1$) or the Stokes limit (Reynold's number $\rightarrow 0$), the resonant frequency in fluid f_{fluid} and quality factor (Q) of the first flexural mode can be calculated from

$$f_{\text{fluid}} = f_0\left[1 + \frac{\pi\rho_f w}{4\rho_c t}\Gamma_{\text{real}}(\text{Re},\kappa)\right]^{-0.5}, \tag{23}$$

$$Q = \frac{\frac{4\rho_c t}{\pi\rho_f w} + \Gamma_{\text{real}}(\text{Re},\kappa)}{\Gamma_{\text{imag}}(\text{Re},\kappa)}, \tag{24}$$

where ρ_f is the fluid density and the complex number Γ is the normalized hydrodynamic force, also referred to as the hydrodynamic function. The hydrodynamic force affects the dynamics of the cantilever by both the added mass and damping of the fluid. A lookup table for Γ is provided in Ref. 36 in terms of the normalized Reynold's number, $\text{Re} = 2\pi f \rho_f w^2/\eta$, where f is the frequency, and the normalized mode number, $\kappa = C_n w/l$, where C_n is the nth positive root of $1+\cos(C_n)\cosh(C_n)=0$ ($C_n = 1.875$ for $n=1$). Reynold's number can vary over several orders of magnitude depending on the cantilever dimensions while $\kappa < 1$ based on our assumption of $l \gg w$. The model is most accurate for narrow, thin cantilevers when $\text{Re} \ll 1$. The hydrodynamic function lookup table from Ref. 36 is plotted in Fig. 2 for flexural cantilever bending.

The frequency response depends on cantilever dimensions and the fluid environment (Fig. 3). The ideal value of f_{max} relative to f_0 will depend on the application. If we consider a force sensor intended for feedback control, the cantilever frequency response up to f_{max} should be relatively flat. In order to simplify the analysis here, we conservatively maintain $f_0 \geq 5 f_{\text{max}}$.

E. Power dissipation

For a constant bias voltage across the Wheatstone bridge, V_{bridge}, half of the potential drop occurs across each resistor (Fig. 1) and the electrical power dissipated in each resistor is

$$W = \frac{(V_{\text{bridge}}/2)^2}{R} = \frac{V_{\text{bridge}}^2}{4R}. \tag{25}$$

The heat is dissipated via convection to the immersing fluid directly from the cantilever and via conduction through the bulk of the silicon device. Excessive power dissipation will increase the temperature of the piezoresistor, leading to a reduced piezoresistive coefficient, increased thermal noise, and potential damage to sensitive samples. For certain applications (e.g., biological force probes), the temperature of the cantilever tip should be only a few degrees above ambient, whereas for other applications (e.g., scanning probe microscopy), the temperature might be limited by other effects such as delamination of the silicon device from the experimental fixture. The relationship between temperature rise and power

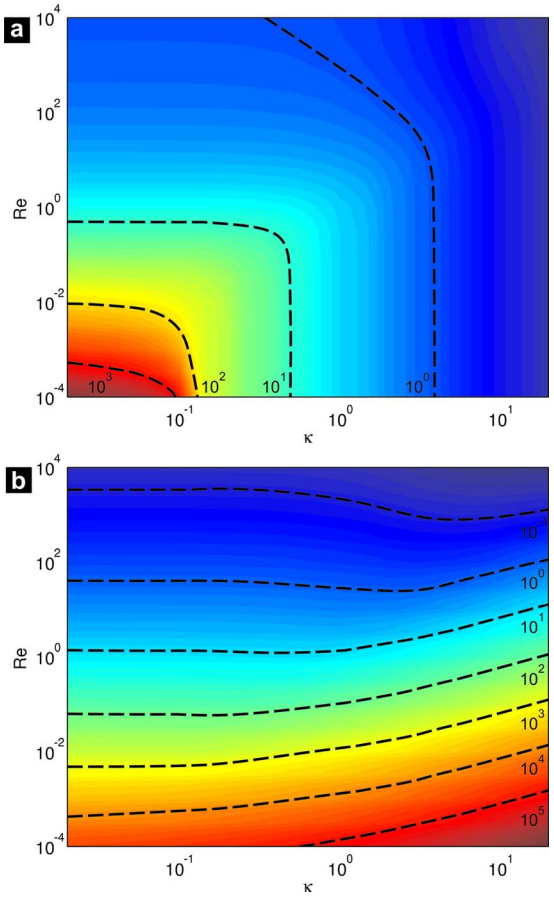

FIG. 2. (Color online) Cantilever hydrodynamic function after the tabulated lookup table in Van Eysden and Sader (Ref. 36). The (a) real (Γ_{real}) and (b) imaginary (Γ_{imag}) parts are plotted with constant Γ contour lines for flexural cantilever bending modes. The resonant frequency and quality factor are calculated from Γ during design optimization for fluid operation applications.

dissipation depends on the cantilever design, but the temperature can be >100 °C for power dissipations as low as 5 mW.[19] To simplify the analysis we apply a power dissipation constraint rather than a temperature constraint, although a simple thermal model could be integrated into the design process in the future.

F. Iterative optimization

As described in the previous sections, cantilever force resolution can be approximated from a set of design parameters which determine the cantilever dimensions, piezoresistor dimensions, dopant profile, and bias voltage. For a typical force sensing application the time resolution and measurement duration are known which determines f_{min} and f_{max}, and the goal is to optimize the force resolution given fabrication and experimental constraints.

Prior analyses of cantilever design have focused on optimizing one or two design parameters at a time with respect to fixed values of the other parameters.[13,37] However, due to the degree of parameter coupling, this approach does not typically find the global optimum.

We implemented an iterative optimization scheme in MATLAB (Mathworks, Cambridge, MA) using fmincon, a gradient based nonlinear optimization algorithm implementing nonlinear constraints. The solution is found iteratively using the L-BFGS-B method,[38] a quasi-Newtonian optimization method; the goal function (e.g., force resolution) is computed for the current design parameters, the parameter change which most rapidly minimizes the goal function is found, and the design parameters are updated before repeating the cycle until the solution converges. Calculation time depends on the computer hardware and model complexity, but takes less than a minute on the hardware that we have tested.

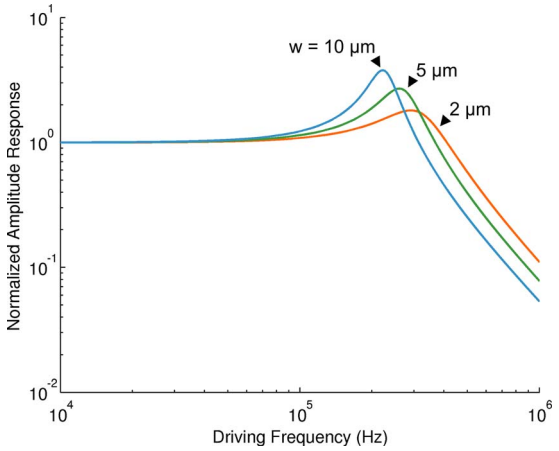

FIG. 3. (Color online) Frequency response in water for 50 μm long, 1 μm thick cantilevers of varying width. The response is approximated by a second order mechanical system with calculated damped natural frequencies of 318, 270, and 226 kHz and quality factors of 1.7, 2.7, and 3.8. A critically damped system ($Q=\sqrt{2}$) is desirable for broadband force sensing to maximize the available flat sensitivity bandwidth and maintain stability in closed-loop systems.

The piezoresistive cantilever design problem is not convex, which we verified by calculating the Hessian matrix for the force resolution. Thus, the local optimum found by the optimizer is not guaranteed to be the global optimum. We investigated the convergence of the optimizer by finding the local optimum for a large number ($>10^5$) of initial randomly generated starting points and found that the global optimum is found more than 99% of the time. This suggests that the global optimum is found in practice (Fig. 4), and the high probability of success means that we are virtually guaranteed to find the global optimum by repeating the optimization routine several times with random starting conditions.

For most calculations we chose to use boron as the dopant atom and the cantilever is accordingly oriented in the ⟨110⟩ direction, which determines the piezoresistive coefficient and elastic modulus. The following constraints were also applied unless otherwise noted in the text:

- $f_{min}=1$ Hz,
- $W\leqslant 2.5$ mW,
- $f_0\geqslant 5f_{max}$,
- $V_{bridge}\leqslant 10$ V,
- $n\leqslant 4.4\times 10^{19}$ cm^{-3},
- $t\geqslant 1$ μm,
- $w\geqslant 2t$.

Several of the constraints (f_{min}, W, n, t) were chosen to closely match previous design optimization work presented

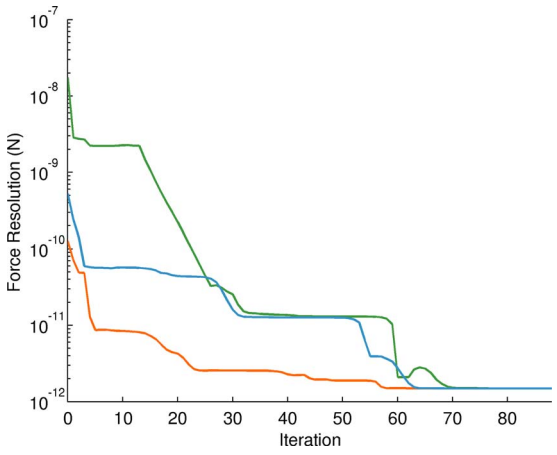

FIG. 4. (Color online) Force resolution improves as the optimizer iterates. At each iteration, the Hessian of the system is numerically approximated and the state variables are updated to move in the direction of steepest descent for the optimization goal. If the constraints are no longer satisfied after a step, the force resolution may increase as the optimizer attempts to satisfy the constraints again.

in Ref. 10. The maximum dopant concentration is based on the solid solubility limit of boron in silicon at 800 °C from Refs. 39 and 40, which are used in modeling packages such as TSUPREM4 (Synopsys, Mountain View, CA). The constraint on $f_0/f_{\max}$ was chosen to maintain a flat frequency response up to $f_{\max}$. The maximum bias voltage was chosen to represent the range of voltages achievable with widely available laboratory power supplies. The ratio of w/t was chosen to ensure that the cantilever is significantly stiffer in plane than out of plane. No constraints were placed upon cantilever stiffness or piezoresistor dimensions, although certain applications may require them.

III. RESULTS AND DISCUSSION

Using the iterative optimization approach presented in Sec. II, we investigated the impact of design choices on cantilever performance.

A. Measurement bandwidth

An increase in measurement bandwidth $f_{\max}$ has two effects on force resolution. First, the resonant frequency of the cantilever must increase so the beam will become shorter and/or thicker, reducing its force sensitivity. Second, the integrated noise increases with $f_{\max}$. Thus, the minimum detectable force increases with measurement bandwidth [Fig. 5(a)].

The optimal piezoresistor design $(l_{\mathrm{pr}}/l, t_{\mathrm{pr}}/t)$ varies continuously with the measurement bandwidth and the constraints applied [Fig. 5(b)]. For the particular constraints used here, t_{pr}/t is initially 1/3 at low frequency. As $f_{\max}$ increases it is beneficial to reduce the resistance (V_J), which increases the dissipated power. Once the power dissipation constraint is reached [Fig. 5(c)], t_{pr}/t decreases while l_{pr}/l increases. At high frequency, another discontinuity is encountered when the optimal bias voltage decreases below the voltage constraint applied. A ratio of $t_{\mathrm{pr}}/t=1/3$ was derived by Harley[10] for the case of an epitaxial piezoresistor with no

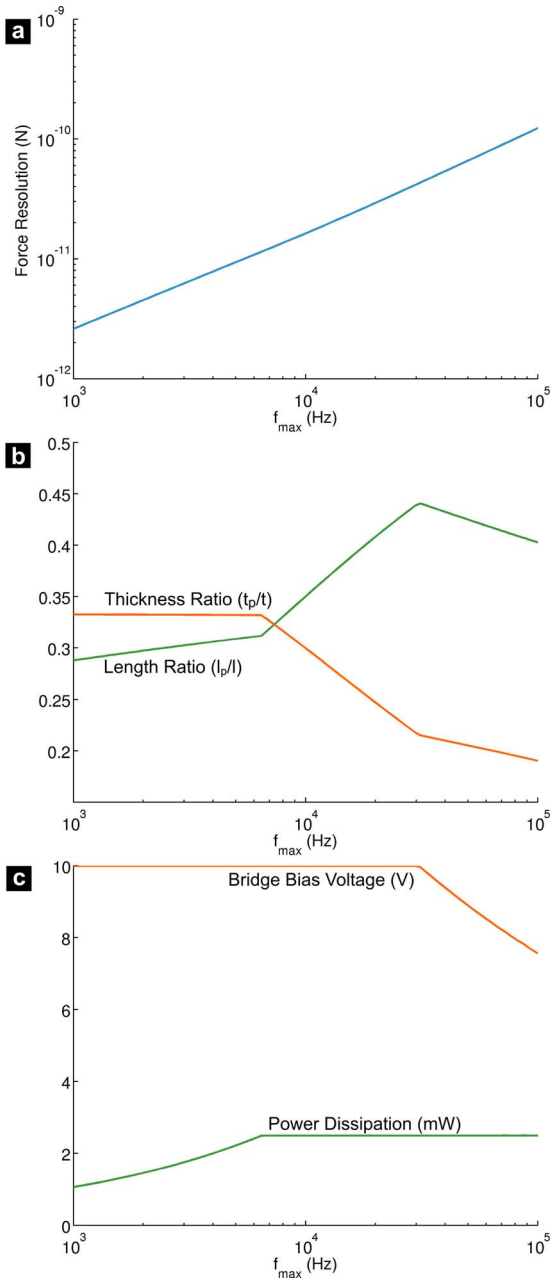

FIG. 5. (Color online) (a) Force resolution, (b) piezoresistor length and thickness ratios, and (c) power dissipation and bias voltage. Results are plotted for optimal designs generated with $f_{\min}=1$ Hz and $f_{\max}$ between 1 and 100 kHz. The cantilever width and thickness are at their lower bound (1 and 2 μm) for all conditions. As $f_{\max}$ increases, the cantilever decreases in length in order to maintain $f_0 \geq 5 f_{\max}$, reducing sensitivity. The piezoresistor becomes thinner and longer relative to the length of the beam, although it becomes shorter in absolute terms due to the shortening of the entire cantilever. For low frequency operation the cantilever is bias voltage constrained $(V_{\mathrm{bridge}}=V_{\mathrm{bridge,max}}$ and $W<W_{\max})$, while at high frequency the cantilever is power dissipation constrained $(W=W_{\max}$ and $V_{\mathrm{bridge}}<V_{\mathrm{bridge,max}})$. The kinks in (b) correspond to the power and voltage limits shown in (c).

constraints on power dissipation or bias voltage, which we clearly observe, however, power dissipation and voltage constraints significantly change the optimal design. Several designs are described in more detail in Table I. The optimal dopant concentration and junction depth are based on a tradeoff between sensitivity and noise subject to the set of constraints applied, particularly power dissipation. As the

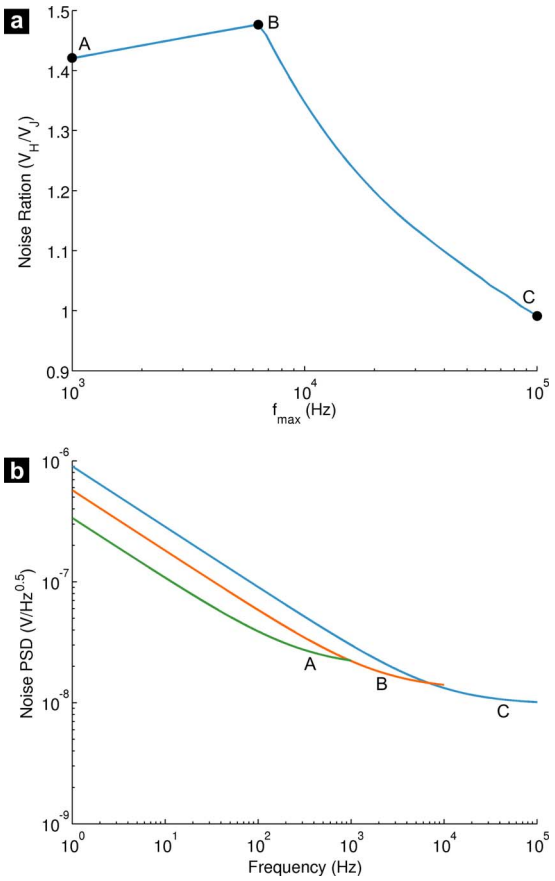

FIG. 6. (Color online) (a) The ratio of Johnson noise to Hooge noise varies f_{max} and the operating constraints but remains on the order of unity in order to maximize the benefit of the two noise sources being uncorrelated. (b) The noise power spectral densities for the three optimized cantilever designs for f_{max} equal to 1, 10, and 100 kHz. The amplifier noise is an order of magnitude less than the piezoresistor noise at all frequencies.

cantilever thickness increases, a thinner, lower concentration piezoresistor is favored (compare cantilevers 1 and 2 in Table I).

B. Balancing the noise

Prior publications have noted that Hooge noise dominates at low frequencies and Johnson noise at high frequencies. However, the contribution of each is dependent on the $1/f$ corner frequency relative to f_{min} and f_{max}, and the corner can be designed as low as 1 Hz or higher than 10 kHz (Ref. 34) by adjusting the number of carriers (N) in the resistor and its resistance (R).

Our results show that the force resolution is optimized when the integrated Hooge voltage noise is comparable to the integrated Johnson voltage noise ($\overline{V_J} \approx \overline{V_H}$) as seen in Fig. 6(a). This result stems from the fact that the Johnson and Hooge noise sources are uncorrelated and the magnitude of the noise is the vector sum of the independent sources. An improvement in force sensitivity is accompanied by an increase in noise; for example, increasing S by reducing t_{pr} and increasing l_{pr} maintains constant N ($\overline{V_H}$) but increases R ($\overline{V_J}$). Thus the change in sensitivity with respect to total noise is maximized when each component of the noise vector is approximately equal. Another interpretation of matching $\overline{V_J}$ and $\overline{V_H}$ is that at frequencies where one is dominant the other is negligible. In other words, below the $1/f$ corner frequency there is effectively no Johnson noise and above it there is no $1/f$ noise. The total system noise is minimized when it is distributed equally between the two [Fig. 6(b)]. The optimal noise ratio ($\overline{V_H}/\overline{V_J}$) varies depending on the operating constraints applied, particularly power consumption, and is analytically investigated in Ref. 26. In previous work, it has not been uncommon to operate the cantilever with a noise ratio of 100:1 or greater[13] which leads to suboptimal performance.

The practical significance of this is that the optimal cantilever design is noisier than expected, making characterization and signal conditioning significantly faster and easier. To characterize the $1/f$ noise properties of a piezoresistor fabrication process it is necessary to measure the noise spectrum and extract α. Measurement time is inversely proportional to the lower bound of the measurement frequency range, so a high corner frequency (e.g., >1 kHz) enables rapid characterization. Additionally, in cases where the $1/f$ noise of the piezoresistor is less than that of the instrumentation amplifier it is necessary to use an ac modulation technique.[34] Based on our results, the optimal piezoresistor design has greater $1/f$ noise than the instrumentation amplifier for many applications and the measurement electronics can use a simple dc bias configuration. We optimized cantilevers for several commercial instrumentation amplifiers to explore the effect of system noise on cantilever design (Table II). As the amplifier noise increases, the optimal piezoresistor becomes

TABLE II. Optimized p-type epitaxial piezoresistive cantilevers for several choices of instrumentation amplifier. Optimization was performed for operation from 1 Hz to 50 kHz with a minimum thickness of 1 μmW, and maximum bias voltage of 10 V. Three amplifiers were considered: TI INA103, AD622, and AD623. The amplifiers were chosen to represent several price points and noise levels. Although the integrated noise of the AD622 and AD623 are 3 times and 17 times greater than that of the INA103, the minimum detectable force only increases by 10% and 70%, respectively. As the instrumentation amplifier noise increases, the piezoresistor is made shorter and thinner, which increases the sensitivity, while the increased $1/f$ noise due to the reduction in N negligibly affects the overall noise while it is less than the amplifier noise.

Cantilever	1	2	3
Amplifier	INA103	AD622	AD623
f_{min} (Hz)	1	1	1
f_{max} (kHz)	50	50	50
l (μm)	74	74	74
w (μm)	2	2	2
t (μm)	1	1	1
l_{pr}/l	0.33	0.31	0.21
t_{pr}/t	0.25	0.23	0.16
n (cm^{-3})	4.4×10^{19}	4.4×10^{19}	4.4×10^{19}
F_{min} (pN)	134	147	230
S_F (V/N)	3.2×10^{4}	3.3×10^{4}	3.8×10^{4}
β^*	0.38	0.39	0.43
$\overline{V_{noise}}$ (V)	4.3×10^{-6}	4.9×10^{-6}	8.8×10^{-6}
$\overline{V_J}$	2.9×10^{-6}	2.9×10^{-6}	2.9×10^{-6}
$\overline{V_H}$	3.1×10^{-6}	3.4×10^{-6}	4.9×10^{-6}
$\overline{V_A}$	4.0×10^{-7}	2.0×10^{-6}	6.7×10^{-6}
f_{corner} (kHz)	5.5	6.5	13.5
N	5.5×10^{8}	4.7×10^{8}	2.2×10^{8}

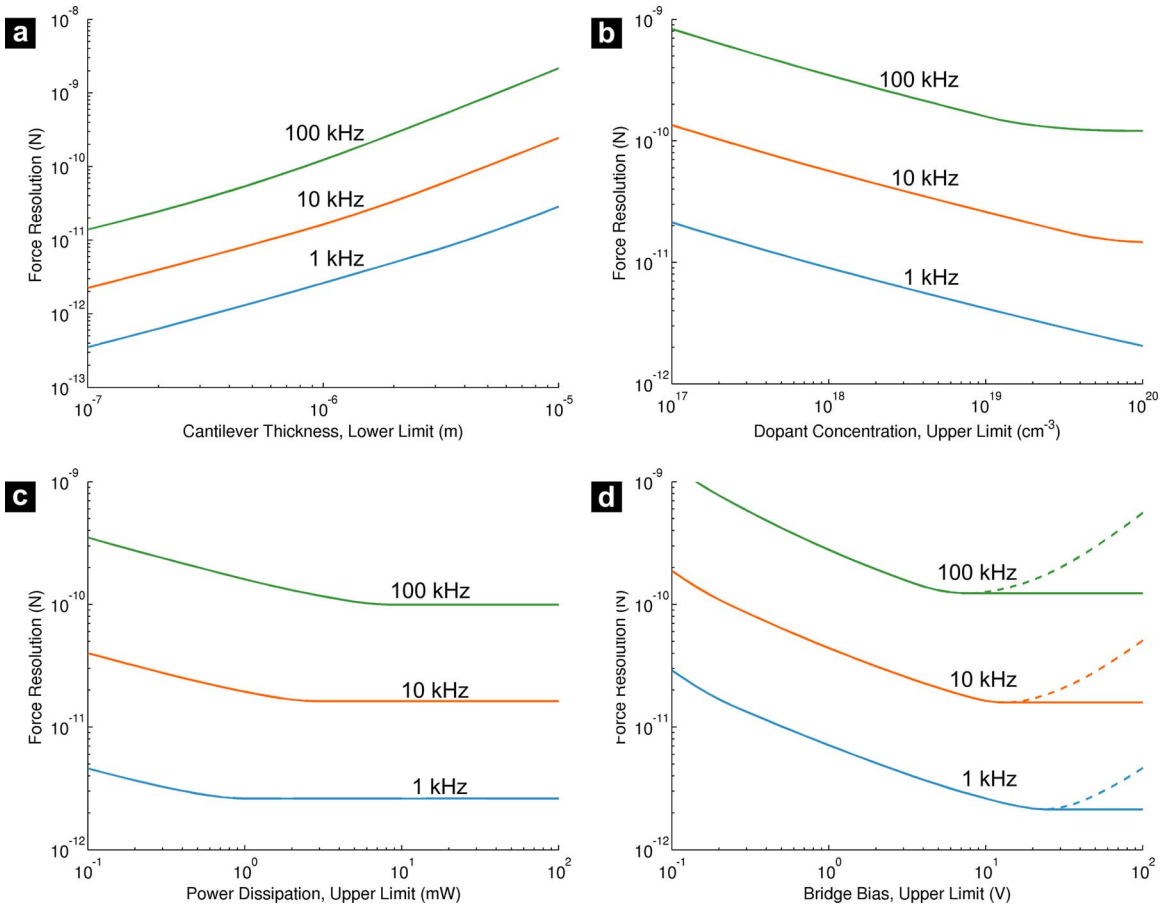

FIG. 7. (Color online) The effect of design constraints on epitaxial piezoresistor force resolution. For all plots, f_{min}=1 Hz while f_{max} is 1, 10, or 100 kHz. (a) Thickness affects force resolution in a straightforward manner and a thinner device is always desirable. (b) The constraint on maximum dopant concentration shows a threshold concentration above which performance is not improved. The concentration threshold is inversely proportional to f_{max}. (c) Force resolution also improves with power dissipation up to a thresold value, above which performance is limited by other constraints (e.g., bias voltage). (d) Although performance improves as the bias voltage constraint is increased (solid line), when the design is forced to have a particular bias voltage (dashed line) performance actually decreases. Thus, applying constraints rather than forcing the cantilever parameters to particular values leads to a more robust design process.

shorter and thinner, which increases the sensitivity. The increased $1/f$ noise due to the smaller number of carriers is negligible compared to the amplifier noise, so the force resolution is improved.

C. Effect of constraints

The design and operation constraints of the cantilever have a significant effect on force resolution [Fig. 7(a)]. Certain constraints, such as thickness, have a continuous effect upon device performance; a thinner cantilever will always perform better than a thicker one for an epitaxial piezoresistor (although not necessarily for an ion implanted piezoresistor). However, other constraints such as the upper dopant concentration limit [Fig. 7(b)], power dissipation limit [Fig. 7(c)], and bias voltage limit [Fig. 7(d)] only improve performance up to a threshold value. This threshold behavior is due to coupling between the constraints; for example, if a cantilever is already dissipating the maximum allowable power, then increasing the voltage is unlikely to be beneficial. The threshold constraint value depends on the measurement bandwidth as well, as seen in Fig. 7(c) where the 1 kHz cantilever achieves optimal performance at a lower power dissipation than the 100 kHz cantilever because of the increased importance of Johnson noise for high frequency operation.

In Fig. 7(d), cantilever performance is optimized with regards to bias voltage for two cases: an upper limit and a fixed value. When the bias voltage is directly fixed, performance suffers as the voltage is increased above the optimal value. When the bias voltage is indirectly set by using a constraint, ideal performance is achieved even when a greater bias voltage is possible. A benefit of the iterative, computated optimization method is that constraints are utilized rather than fixed parameter values, leading to improved performance and a more robust, user-friendly design process.

D. Operation in water

Operating a cantilever in liquid rather than air reduces the resonant frequency and quality factor. For control stability, a lower quality factor can be desirable, but the cantilever must be made shorter in order to maintain the same first resonant mode frequency. A comparison of water and air performance is presented in Fig. 8. Performance is reduced slightly in water, particularly as cantilever width is increased.

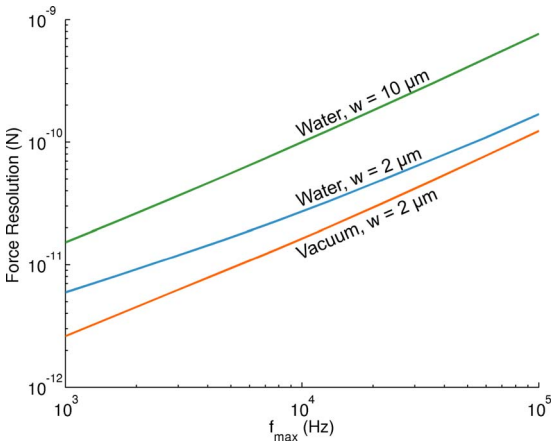

FIG. 8. (Color online) Force resolution comparison between cantilevers optimized for operation in vacuum and in water for varying f_{max}. In the latter case, fluid damping reduces the natural frequency and quality factor of the cantilever, necessitating a reduction in length to maintain the same resonant frequency. The effect is pronounced for high frequency operation and for wider cantilevers.

E. Choice of dopant type and concentration

Dopant concentration affects the piezoresistive coefficient, sensitivity to temperature fluctuations, number of carriers, and resistance, thus affecting both sensitivity and noise. Increasing the number of carriers with fixed resistor dimensions decreases both Johnson and Hooge noise by decreasing R and increasing N. However, it also leads to a reduction in the piezoresistive coefficient and increases the power consumption for a fixed bias voltage. For thin cantilevers (e.g., 1 μm thick), performance is optimized when the dopant concentration is made as large as possible, constrained by the solid solubility limit of the dopant atom. However, the optimal dopant concentration decreases in a number of cases, such as when cantilever thickness is increased (Table I).

Although the piezoresistive coefficient for n-type silicon in the ⟨100⟩ direction (103×10^{-11} Pa^{-1}) is higher than p-type silicon in the ⟨110⟩ direction (72×10^{-11} Pa^{-1}) at low concentrations,[22] the elastic modulus of silicon in the ⟨100⟩ direction is 130 GPa, as compared to 169 GPa in the ⟨110⟩ direction. As noted earlier, sensitivity is independent of elastic modulus, whereas natural frequency is not. Thus, for a fixed natural frequency a n-type cantilever must be shorter and/or thicker than an equivalent p-type cantilever to compensate for its lower modulus, resulting in a modest performance advantage of 10% for a fixed dopant concentration.

However, there are several potential benefits to choosing a n-type rather than a p-type piezoresistor. First, the solid solubility limit of phosphorus is approximately an order of magnitude larger than that of boron at typical processing temperatures.[39,40] This leads to a $>10\%$ performance advantage for n-type piezoresistors when a high dopant concentration is favored (Table III). Second, the increased thickness of a n-type cantilever to maintain a fixed natural frequency is beneficial during fabrication. Finally, arsenic has a significantly lower diffusivity in silicon than boron or phosphorus and enables the formation of a shallow piezoresistor with enough postanneal time to minimize α, as discussed in Ref. 1. Historically, p-type piezoresistors may have been dominant because they are straight forward to release using anisotropic wet etches (e.g., KOH and TMAH), but the current wide availability of deep reactive ion etching and silicon-on-insulator wafers makes both p-type and n-type cantilevers straightforward to fabricate.

TABLE III. Optimized p- and n-type epitaxial piezoresistive cantilevers. Optimization was performed for operation from 1 Hz to 50 kHz with a minimum thickness of 1 μm, maximum power dissipation of 2.5 mW, and maximum bias voltage of 10 V. The minimum detectable force of the p-type piezoresistor is 40% larger than that of the n-type piezoresistor.

Cantilever	1	2
Dopant	Boron	Phosphorus
f_{min} (Hz)	1	1
f_{max} (kHz)	50	50
l (μm)	74	69
w (μm)	2	2
t (μm)	1	1
l_{pr}/l	0.33	0.36
t_{pr}/l	0.25	0.17
n (cm^{-3})	4.4×10^{19}	1.0×10^{20}
F_{min} (pN)	134	96
S_F (V/N)	3.2×10^{4}	2.8×10^{4}
β^*	0.38	0.36
$\overline{V_{noise}}$ (V)	4.3×10^{-6}	2.7×10^{-6}
$\overline{V_H}/\overline{V_J}$	1.1	0.86
f_{corner} (kHz)	5.5	3.5
N	5.5×10^{8}	8.7×10^{8}
k (N/m)	0.21	0.19
f_0 (kHz)	250	250
f_{fluid} (kHz)	130	130
V_{bridge} (V)	10	7.0
R (kΩ)	10	5.0
W (mW)	2.5	2.5

F. Generalization

To demonstrate the generality of our design method, we extended the code to handle diffusion doping. Diffusion was implemented by generating a dopant concentration profile as a function of furnace time and temperature, rather than simply concentration and thickness as in the case of epitaxy. The diffusion model is based on Ref. 41 and was verified with spreading resistance (Solecon Laboratories, Reno, NV) for a $POCl_3$ diffusion process [Fig. 9(a)]. The diffusion model we used importantly captures the kink and tail of the phosphorus profile.

The performance of diffusion and epitaxy designs were compared for a single case [Fig. 9(b)]. Both the designs used n-type (phosphorus) piezoresistors in contrast with the p-type (boron) results presented elsewhere in the paper and were optimized for operation between 1 Hz and 1 kHz with a minimum cantilever thickness of 1 μm and maximum power dissipation of 3.5 mW. The force resolution for the epitaxy ($R_s=19.5\ \Omega$, $N_z=5.49\times10^{7}$ cm^{-2}) and diffusion ($R_s=26.2\ \Omega$, $N_z=3.50\times10^{7}$ cm^{-2}) designs are 1.3 and 1.5 pN, respectively. Clearly the optimal junction depth for the epitaxial piezoresistor is significantly less than for the diffused piezoresistor; in the latter case, the entire cantilever is doped.

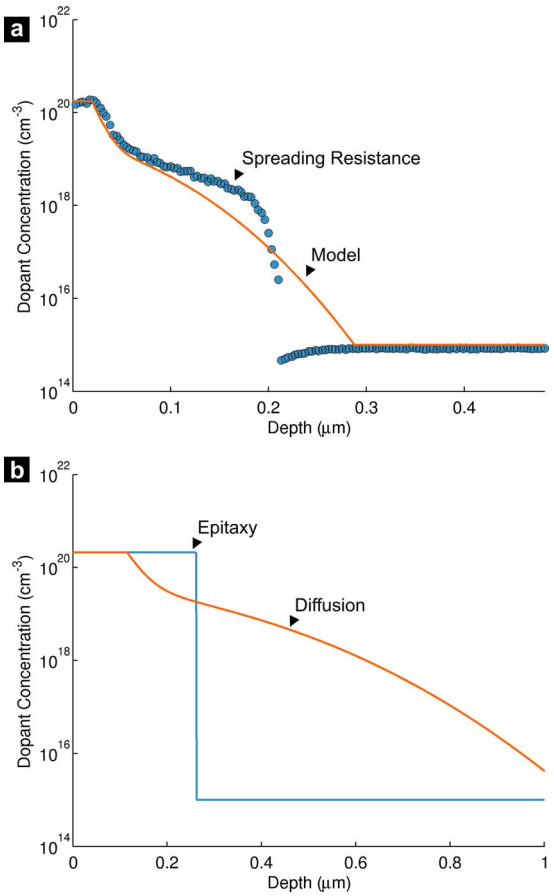

FIG. 9. (Color online) (a) A dopant profile model is required for the design of diffusion based piezoresistors. We performed a low temperature (800 °C) $POCl_3$ diffusion and found the dopant profile by spreading resistance analysis, which compared well with a diffusion model in the literature. (b) We then compared the optimal dopant profile for epitaxy and diffusion cantilevers. The optimal diffusion junction depth is significantly greater than the epitaxy junction depth, thus extrapolating epitaxial piezoresistor design rules (e.g., $t_{pr}/t=1/3$) to other doping processes can be problematic. Comparable force resolution is obtained with both fabrication processes.

Other extensions such as resonant force sensing, a detailed thermal model, and ion implantation would be straightforward to implement in the future by direct calculation or by integration with a finite element analysis or process simulation tool.

IV. CONCLUSIONS

We have presented a general iterative optimization technique for the design of piezoresistive force sensors and presented results for the optimization of a broadband force sensor. In summary, the optimal cantilever design strongly depends on the frequency content of the signal and design constraints. One benefit of iterative optimization is that constraints are applied as bounds rather than fixed parameter values, leading to a more robust, user-friendly design process. We demonstrated that the common choice of $t_{pr}/t=1/3$ is not generally optimal when design and operation constraints are considered (e.g., power dissipation, bias voltage) and when nonuniform dopant concentration profiles are introduced (e.g., ion implantation, diffusion). In general, optimal performance is obtained when the integrated Johnson noise and $1/f$ noise are approximately equal. We have focused on epitaxial piezoresistors here, but have also demonstrated the generality of the method by extending the method to diffusion doping.

ACKNOWLEDGMENTS

Fabrication work was performed in part at the Stanford Nanofabrication Facility (a member of the National Nanotechnology Infrastructure Network) supported by the NSF under Grant No. ECS-9731293, its laboratory members, and the industrial members of the Stanford Center for Integrated Systems. This work was supported by the National Institutes of Health under Grant No. EB006745 and the National Science Foundation (NSF) under CAREER Award Nos. ECS-0449400 and COINS NSF-NSEC ECS-0425914. J.C.D. was supported in part by a National Defense Science and Engineering Graduate (NDSEG) Fellowship and a NSF Graduate Research Fellowship. S.-J.P. was supported by a Samsung fellowship. The authors would like to thank Nahid Harjee, Bryan Petzold, and Ali Rastegar for helpful discussions.

APPENDIX: OPTIMIZATION CODE

The cantilever optimization code used in this paper is open source, written in object oriented MATLAB, and freely available at http://microsystems.stanford.edu/piezoD. It requires MATLAB R2008a or newer and the optimization toolbox.

[1] G. Villanueva, J. Plaza, J. Montserrat, F. Perez-Murano, and J. Bausells, Microelectron. Eng. **85**, 1120 (2008).
[2] S.-J. Park, M. B. Goodman, and B. L. Pruitt, Proc. Natl. Acad. Sci. U.S.A. **104**, 17376 (2007).
[3] G. Binnig, C. F. Quate, and C. Gerber, Phys. Rev. Lett. **56**, 930 (1986).
[4] F. T. Goericke and W. P. King, IEEE Sens. J. **8**, 1404 (2008).
[5] M. Tortonese, R. C. Barrett, and C. F. Quate, Appl. Phys. Lett. **62**, 834 (1993).
[6] A. Barlian, W.-T. Park, J. Mallon, A. Rastegar, and B. Pruitt, Proc. IEEE **97**, 513 (2009).
[7] S. C. Minne, J. D. Adams, G. Yaralioglu, S. R. Manalis, A. Atalar, and C. F. Quate, Appl. Phys. Lett. **73**, 1742 (1998).
[8] R. P. Ried, H. J. Mamin, B. D. Terris, L. S. Fan, and D. Rugar, Solid State Sensors and Actuators **1**, 447 (1997).
[9] C. Hagleitner, A. Hierlemann, D. Lange, A. Kummer, N. Kerness, O. Brand, and H. Baltes, Nature (London) **414**, 293 (2001).
[10] J. Harley and T. Kenny, J. Microelectromech. Syst. **9**, 226 (2000).
[11] X. Yu, J. Thaysen, O. Hansen, and A. Boisen, J. Appl. Phys. **92**, 6296 (2002).
[12] E. Chow, H. Soh, H. Lee, J. Adams, S. Minne, G. Yaralioglu, A. Atalar, C. Quate, and T. Kenny, Sens. Actuators, A **83**, 118 (2000).
[13] Z. Wang, R. Yue, R. Zhang, and L. Liu, Sens. Actuators, A **120**, 325 (2005).
[14] M. Papila, R. Haftka, T. Nishida, and M. Sheplak, J. Microelectromech. Syst. **15**, 1632 (2006).
[15] M. Liu, K. Maute, and D. M. Frangopol, Reliab. Eng. Syst. Saf. **92**, 1333 (2007).
[16] T. Duc, J. Creemer, and P. Sarro, IEEE Sens. J. **7**, 96 (2007).
[17] J. Creemer, F. Fruett, G. Meijer, and P. French, IEEE Sens. J. **1**, 98 (2001).
[18] M. Doelle, D. Mager, P. Ruther, and O. Paul, Sens. Actuators, A **127**, 261 (2006).
[19] F. Goericke, J. Lee, and W. P. King, Sens. Actuators, A **143**, 181 (2008).
[20] R. Roark and W. Young, *Formulas for Stress and Strain* (McGraw-Hill, New York, 1975).
[21] J. Chen and N. MacDonald, Rev. Sci. Instrum. **75**, 276 (2004).
[22] Y. Kanda, IEEE Trans. Electron Devices **29**, 64 (1982).
[23] J. Richter, J. Pedersen, M. Brandbyge, E. Thomsen, and O. Hansen, J. Appl. Phys. **104**, 023715 (2008).
[24] J. A. Harley and T. W. Kenny, Appl. Phys. Lett. **75**, 289 (1999).

[25]M. Tortonese, "Force sensors for scanning probe microcopy," Ph.D. dissertation, Stanford University, 1993.
[26]S.-J. Park, A. Rastegar, T. Fung, A. Barlian, J. Mallon, and B. Pruitt, "Optimization of piezoresistive cantilever performance," Hilton Head Sensors, Actuators and Microsystems Workshop, 2008), p. 3.
[27]T. Gabrielson, U. Center, and P. Warminster, IEEE Trans. Electron Devices **40**, 903 (1993).
[28]O. Hansen and A. Boisen, Nanotechnology **10**, 51 (1999).
[29]M. R. Paul, M. T. Clark, and M. C. Cross, Nanotechnology **17**, 4502 (2006).
[30]J. Arlett, J. Maloney, B. Gudlewski, and M. Muluneh, Nano Lett. **6**, 1000 (2006).
[31]S. Senturia, *Microsystem Design* (Springer, Berlin, 2000).
[32]G. Masetti, M. Severi, and S. Solmi, IEEE Trans. Electron Devices **30**, 764 (1983).
[33]F. Hooge, IEEE Trans. Electron Devices **151**, 3 (1994).
[34]J. Mallon, A. Rastegar, A. Barlian, M. Meyer, T. Fung, and B. Pruitt, Appl. Phys. Lett. **92**, 3508 (2008).
[35]A. Partridge, "Lateral piezoresistive accelerometer with epipoly encapsulation," Thesis, Stanford University, 2003.
[36]C. A. van Eysden and J. E. Sader, J. Appl. Phys. **104**, 109901 (2007).
[37]C. Pramanik, H. Saha, and U. Gangopadhyay, J. Micromech. Microeng. **16**, 2060 (2006).
[38]C. Zhu, R. Byrd, P. Lu, and J. Nocedal, ACM Trans. Math. Softw. **23**, 550 (1997).
[39]G. Vick and K. Whittle, J. Electrochem. Soc. **116**, 1142 (1969).
[40]F. Trumbore, *Micro and Thin-film Electronics: Readings* (Holt, Rinehart, and Winston, New York, 1964), p. 177.
[41]J. Tsai, Proc. IEEE **57**, 1499 (1969).